Chapter 7.

MULTIVARIABLE OPTIMAL CONTROL

7.1. Applications of Multilevel Converters

Multilevel converters can be used for many different medium- and high-power applications. Since these converters are reversible, they can operate either as inverters or as rectifiers. Some examples of practical applications for these systems are:

- Electricity generation plants. The electric energy produced by these plants must be injected into the electrical grid. The DC-link of the converter receives electric energy in DC form, and the AC side of the converter is connected to the utility. Some practical applications include renewable energies such as photovoltaic panels (Fig. 7.1) or air generators. Air generators usually produce AC voltages; however, these voltages can be converted into DC form, and then into AC form again by means of two multilevel converters connected back-to-back. This process allows the blades of the mill to rotate asynchronously with respect to the utility frequency; hence, the speed can be adjusted such that the generator can achieve maximum efficiency according to wind conditions.

- Boost rectifier. These systems can rectify AC current from the electrical grid operating with high PF [B3]. This application includes the rectifier stage of a motor drive system. Since the converter is reversible in this application, the rectifier allows bi-directional energy flux so that the mechanical energy from the motor can be recovered into the utility.
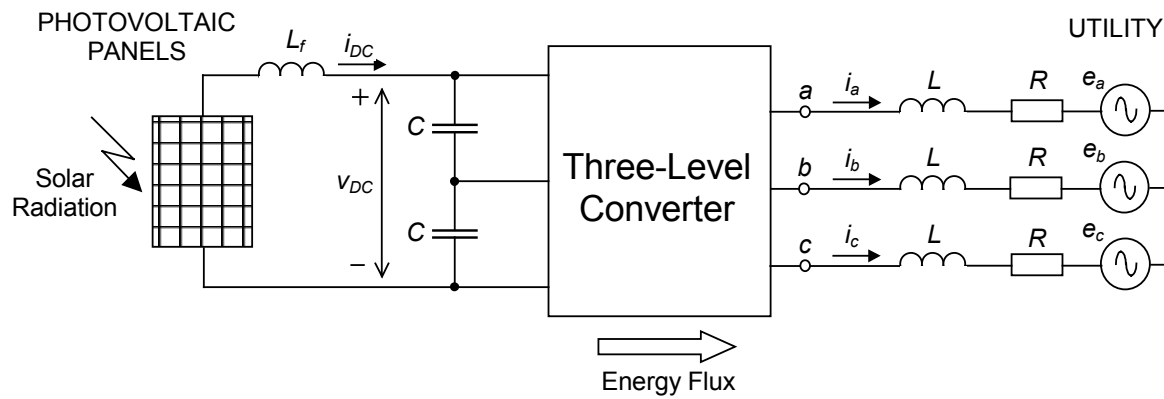
Fig. 7.1. *Multilevel converter applied to renewable energy.*

- SMES systems. The reversibility feature is essential for these systems, since the energy accumulated into the superconducting coil must be recovered into the AC side when it is required [A10].

- High-voltage DC (HVDC) transmission. This alternative becomes economically attractive where a large amount of power is to be transmitted over a long distance from a remote generating plant to the load center. This breakeven distance for HVDC overhead transmission lines usually lies somewhere in a range of 500-600 km and is much smaller for underwater cables. In addition, many other factors, such as the improved transient stability and the dynamic damping of the electrical system oscillations, may influence the selection of DC transmission in preference to the AC transmission. It is possible to interconnect two AC systems, which are at two different frequencies or which are not synchronized, by means of an HVDC transmission line. Multilevel converters are often the suitable solution for synthesizing these systems.

In this chapter, the three-level converter is applied to systems in which the variables to be controlled are the reactive current (i_q) and the DC-link voltage (v_{DC}). For unity PF applications, the reactive current will be defined as zero.

7.2. Proportional-Integral dq Controller

A control diagram for the three-level-based system can be obtained from (2.26). This equation can be also expressed as follows:

$$v_d = \Delta v_d - \omega L\, i_q + E_L \quad \text{and} \quad v_q = \Delta v_q + \omega L\, i_d, \tag{7.1}$$

in which $\Delta v_d = L\dfrac{di_d}{dt} + R\, i_d$ and $\Delta v_q = L\dfrac{di_q}{dt} + R\, i_q$.

The control diagram is pictured in Fig. 7.2, in which the blocks that contain ωL have the objective of decoupling influences between both current control loops [A56]. Nevertheless, due to sensing errors and filtering delays, some practical influences between the loops still remain after decoupling the channels.

The small-signal model of the converter (2.40) can be used for the design of the voltage and current controllers, which are based on proportional and integral (PI) actuations. The parameters of this controller can be calculated by classical design methods. Poles and zeros of the compensators should be located with the objective of achieving good static and dynamic performance of the system, and providing sufficient stability margins.

The design process of this controller is not carried out in this dissertation. The main reason is that it makes use of standard design methods and its discussion would not make any important contribution.
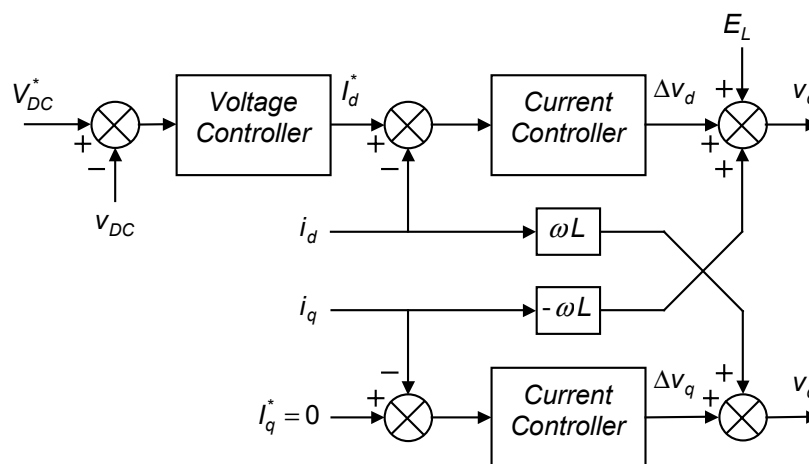
Fig. 7.2. Decoupled PI-dq controller.

7.3. LQR Controller

An optimal control loop will be used for controlling the three-level converter as a boost rectifier. An introduction to the multivariable optimal control is presented in the following.

7.3.1 Introduction to the LQR

Since the multilevel boost rectifier is a MIMO system, an LQR can be applied as a control loop. The objective of this control method is to minimize a quadratic performance index (J) as follows:

$$J = \frac{1}{2}\mathbf{x}^{\mathrm{T}}{}_{(T_N)}\mathbf{M}\,\mathbf{x}_{(T_N)} + \frac{1}{2}\int_0^{T_N} [\mathbf{x}^{\mathrm{T}}{}_{(t)}\mathbf{Q}\,\mathbf{x}_{(t)} + \mathbf{u}^{\mathrm{T}}{}_{(t)}\mathbf{R}\,\mathbf{u}_{(t)}]dt \;, \tag{7.2}$$

in which $\mathbf{M}$, $\mathbf{Q}$ and $\mathbf{R}$ are hermitic weighting matrices positively defined.

The optimal quadratic problem consists of finding a control law $\mathbf{u}_{(t)}$ which achieves the minimum value for J. The system performance is restricted to its state-space equation (7.3), such that:

$$\frac{d}{dt}\mathbf{x}_{(t)} = \mathbf{A}\,\mathbf{x}_{(t)} + \mathbf{B}\,\mathbf{u}_{(t)} \;, \tag{7.3}$$

which is assumed to be a state controllable system.

Because of the digital control used in this application, the analysis will be made from the standpoint of a discrete-time system. Thus, (7.2) and (7.3) must be transformed into discrete equations, as follows:

$$J = \frac{1}{2}\mathbf{x}^{\mathrm{T}}{}_{(N)}\mathbf{M}\,\mathbf{x}_{(N)} + \frac{1}{2}\sum_{k=0}^{N-1}\left[\mathbf{x}^{\mathrm{T}}{}_{(k)}\mathbf{Q}\,\mathbf{x}_{(k)} + \mathbf{u}^{\mathrm{T}}{}_{(k)}\mathbf{R}\,\mathbf{u}_{(k)}\right] \text{ and} \tag{7.4}$$

$$\mathbf{x}_{(k+1)} = \mathbf{A}_d\,\mathbf{x}_{(k)} + \mathbf{B}_d\,\mathbf{u}_{(k)} \;, \tag{7.5}$$

where matrices $\mathbf{A}_d$ and $\mathbf{B}_d$ depend on the discrete time T_m, such that

$$\mathbf{A}_d = e^{\mathbf{A}T_m} \quad \text{and} \quad \mathbf{B}_d = \left(\int_0^{T_m} e^{\mathbf{A}\tau}\,d\tau\right)\mathbf{B} \;. \tag{7.6}$$

$\mathbf{M}$, $\mathbf{Q}$ and $\mathbf{R}$ in (7.4) are symmetric weighting matrices which will be selected by the designer, who bases the choice on the relative importance of the various states and

controls. Some weights are selected according to practical control issues; otherwise the solution would include large components in the control gains, which could saturate the actuator device. The usually diagonal **Q** and **R** matrices require that all elements be either positive or zero.

Minimizing the quadratic performance index J given in (7.4) also called cost function, with the restriction of the discrete state equation (7.5) can be achieved by using Lagrange's multipliers method [B9]. The solution of the optimal control leads to a linear closed loop-control law such that:

$$\mathbf{u}(k) = -\mathbf{K}(k)\,\mathbf{x}(k)\,.$$
(7.7)

The optimal control problem is reduced to find the coefficients of matrix $\mathbf{K}(k)$. If the control actuation time is defined as infinite ($N=\infty$), this matrix becomes constant ($\mathbf{K}(k) = \mathbf{K}$). This is a very important issue, since it allows the LQR control to be easily implemented in practical systems.

All state variables must be available; in other words, the system must be observable, and also, it must be state controllable. An important advantage of using an LQR strategy is that the system becomes asymptotically stable in the steady-state condition [B9, B10]. This is because the objective of this control is to minimize a function that includes all the state-space variables in it.

7.3.2. Control Actuation Delay

Actuation delays are inherent attributes of digital control loops. In general terms, any digital control requires the following steps: sensing analog variables and converting them into digital, processing them according to an established control law and calculation of control signals, and finally, applying those control signals to the system. Additionally, for the case of a PWM power electronics system, the modulation process imposes a delay of an integer number of modulation periods, which is usually one single period in order to guarantee good dynamics for the system. Therefore, all of the tasks should be done within a modulation period, which is the same as the sampling period.

Assuming one single discrete-time delay, the state-space equations can be expressed as:

$$\mathbf{x}(k+1) = \mathbf{A}_d\,\mathbf{x}(k) + \mathbf{B}_d\,\mathbf{u}(k-1) \quad \text{and} \quad \mathbf{y}(k) = \mathbf{C}\mathbf{x}(k)\,.$$
(7.8)

The system should be reformulated into the standard state-space equations so that it can be directly processed by classical analysis and synthesis methods using its internal description. Thus, some new state variables should be defined [B11] to include the delayed control term:

$$\mathbf{x}_u(k) = \mathbf{u}(k-1).$$ (7.9)

The new appearance of the state-space formulation is:

$$\begin{bmatrix} \mathbf{x}(k+1) \\ \mathbf{x}_u(k+1) \end{bmatrix} = \begin{bmatrix} \mathbf{A}_d & \mathbf{B}_d \\ \mathbf{0} & \mathbf{0} \end{bmatrix} \begin{bmatrix} \mathbf{x}(k) \\ \mathbf{x}_u(k) \end{bmatrix} + \begin{bmatrix} \mathbf{0} \\ \mathbf{1} \end{bmatrix} \mathbf{u}(k).$$ (7.10)

Equation (7.10) can be now processed by means of classical methods. Notice that this formulation increases the number of state variables by the same number of control variables.

7.3.3. LQR with Integral Actuation

Fig. 7.3 shows a basic diagram of the LQR. Matrix $\mathbf{K}_{(k)}$ can be calculated either for a finite process (finite N), or for a steady-state process ($N=\infty$). In any case, this matrix can be calculated off-line.
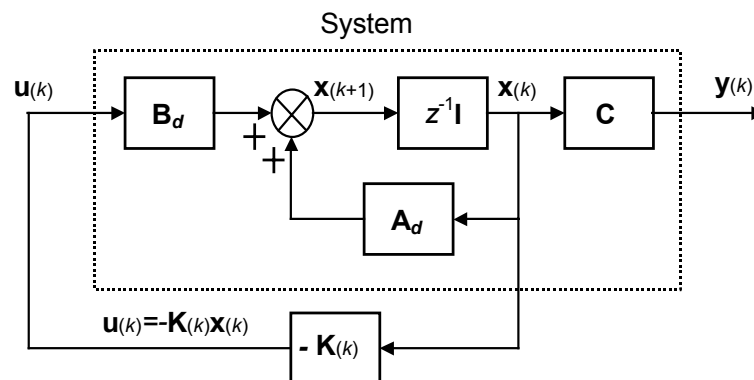
Fig. 7.3. Basic LQR diagram.

By means of the control loop shown in Fig. 7.3, all of the state variables tend to reach zero in accordance with an optimal process. For this case, the references of the output variables are intrinsically defined as zero.

In the control diagram shown in Fig. 7.4, the state variables and the output variables can be defined as non-zero in steady-state conditions. This is achieved thanks to a new external control loop. Additionally, due to the introduction of an integral

actuation in the direct chain, zero-order errors caused by step references or disturbances can be removed in steady-state conditions [A50, B9]. This integral-type optimal regulator is called LQR with integral actuation.
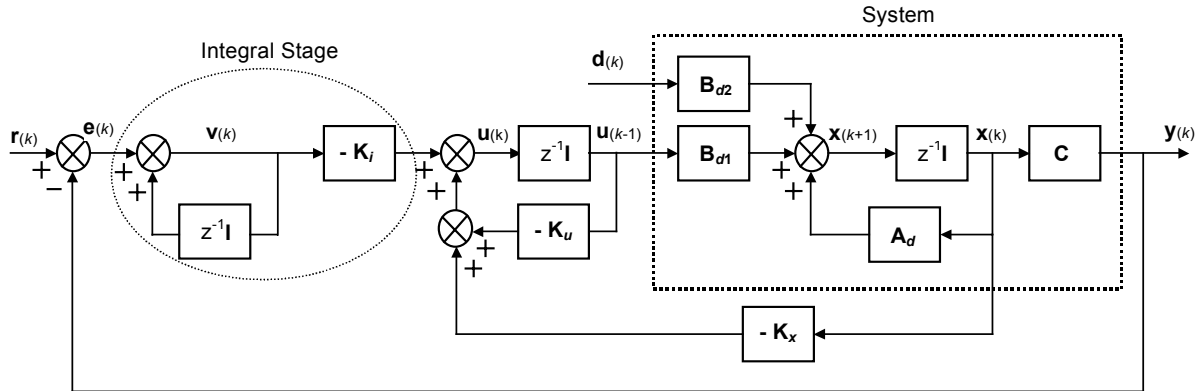

Fig. 7.4. *LQR diagram with integral actuation.*

The control diagram in Fig. 7.4 includes possible system disturbances that can be included in (7.8) as follows:

$$\mathbf{x}(k+1) = \mathbf{A}_d\mathbf{x}(k) + \mathbf{B}_{d1}\mathbf{u}(k-1) + \mathbf{B}_{d2}\mathbf{d}(k) \quad \text{and} \quad \mathbf{y}(k) = \mathbf{C}\,\mathbf{x}(k). \tag{7.11}$$

In order to formulate the dynamic performance of the whole system, including the control diagram, some new state variables should be defined. These variables must be inputs of multiplier blocks **K**, such as the accumulative variables of the integral actuation $\mathbf{v}(k)$:

$$\mathbf{v}(k) = \mathbf{r}(k) - \mathbf{y}(k) + \mathbf{v}(k-1). \tag{7.12}$$

From (7.11) and (7.12):

$$\mathbf{v}(k+1) = -\mathbf{C}\mathbf{A}_d\mathbf{x}(k) + \mathbf{v}(k) - \mathbf{C}\mathbf{B}_{d1}\mathbf{u}(k-1) + \mathbf{r}(k+1) - \mathbf{C}\mathbf{B}_{d2}\mathbf{d}(k). \tag{7.13}$$

These variables are added to the state-space equation:

$$\begin{bmatrix} \mathbf{v}(k+1) \\ \mathbf{x}(k+1) \end{bmatrix} = \begin{bmatrix} \mathbf{I} & -\mathbf{C}\mathbf{A}_d \\ \mathbf{0} & \mathbf{A}_d \end{bmatrix} \begin{bmatrix} \mathbf{v}(k) \\ \mathbf{x}(k) \end{bmatrix} + \begin{bmatrix} -\mathbf{C}\mathbf{B}_{d1} \\ \mathbf{B}_{d1} \end{bmatrix} \mathbf{u}(k-1) + \begin{bmatrix} \mathbf{I} \\ \mathbf{0} \end{bmatrix} \mathbf{r}(k+1) + \begin{bmatrix} -\mathbf{C}\mathbf{B}_{d2} \\ \mathbf{B}_{d2} \end{bmatrix} \mathbf{d}(k). \tag{7.14}$$

For the previous sample period:

$$\begin{bmatrix} \mathbf{v}(k) \\ \mathbf{x}(k) \end{bmatrix} = \begin{bmatrix} \mathbf{I} & -\mathbf{C}\mathbf{A}_d \\ \mathbf{0} & \mathbf{A}_d \end{bmatrix} \begin{bmatrix} \mathbf{v}(k-1) \\ \mathbf{x}(k-1) \end{bmatrix} + \begin{bmatrix} -\mathbf{C}\mathbf{B}_{d1} \\ \mathbf{B}_{d1} \end{bmatrix} \mathbf{u}(k-2) + \begin{bmatrix} \mathbf{I} \\ \mathbf{0} \end{bmatrix} \mathbf{r}(k) + \begin{bmatrix} -\mathbf{C}\mathbf{B}_{d2} \\ \mathbf{B}_{d2} \end{bmatrix} \mathbf{d}(k-1). \tag{7.15}$$

Then, (7.15) is subtracted from (7.14), and the following definitions are taken into account:

$$\Delta \mathbf{v}(k) = \mathbf{v}(k) - \mathbf{v}(k-1),$$

$$\Delta \mathbf{x}(k) = \mathbf{x}(k) - \mathbf{x}(k-1), \text{ and} \tag{7.16}$$

$$\Delta \mathbf{u}(k-1) = \mathbf{u}(k-1) - \mathbf{u}(k-2).$$

Thus, a new state-space representation is obtained, as follows:

$$\begin{bmatrix} \Delta \mathbf{v}(k+1) \\ \Delta \mathbf{x}(k+1) \end{bmatrix} = \begin{bmatrix} \mathbf{I} & -\mathbf{C}\mathbf{A}_d \\ \mathbf{0} & \mathbf{A}_d \end{bmatrix} \begin{bmatrix} \Delta \mathbf{v}(k) \\ \Delta \mathbf{x}(k) \end{bmatrix} + \begin{bmatrix} -\mathbf{C}\mathbf{B}_{d1} \\ \mathbf{B}_{d1} \end{bmatrix} \Delta \mathbf{u}(k-1). \tag{7.17}$$

In this equation, all of the variables tend to be zero in steady-state conditions. The references and disturbances are assumed to be an initial step, and so they disappear when dealing with the difference between two consecutive samples.

If the period delay of the control actuation is also included, the entire state-space formulation is shown according to the standard form:

$$\underbrace{\begin{bmatrix} \Delta \mathbf{v}(k+1) \\ \Delta \mathbf{x}(k+1) \\ \Delta \mathbf{x}_u(k+1) \end{bmatrix}}_{\hat{\mathbf{x}}(k+1)} = \underbrace{\begin{bmatrix} \mathbf{I} & -\mathbf{C}\mathbf{A}_d & -\mathbf{C}\mathbf{B}_{d1} \\ \mathbf{0} & \mathbf{A}_d & \mathbf{B}_{d1} \\ \mathbf{0} & \mathbf{0} & \mathbf{0} \end{bmatrix}}_{\hat{\mathbf{A}}_d} \underbrace{\begin{bmatrix} \Delta \mathbf{v}(k) \\ \Delta \mathbf{x}(k) \\ \Delta \mathbf{x}_u(k) \end{bmatrix}}_{\hat{\mathbf{x}}(k)} + \underbrace{\begin{bmatrix} \mathbf{0} \\ \mathbf{0} \\ \mathbf{I} \end{bmatrix}}_{\hat{\mathbf{B}}_d} \underbrace{\Delta \mathbf{u}(k)}_{\hat{\mathbf{u}}(k)}. \tag{7.18}$$

The term $\Delta \mathbf{x}_u(k)$ in (7.18) is $\Delta \mathbf{u}(k-1)$, in accordance with definition (7.9) in the previous section. On the other hand, the term $\Delta \mathbf{v}(k)$ is, in fact, the error $\mathbf{e}(k)$ from the references and the output variables:

$$\Delta \mathbf{v}(k) = \mathbf{v}(k) - \mathbf{v}(k-1) = \mathbf{r}(k) - \mathbf{y}(k) + \mathbf{v}(k-1) - \mathbf{v}(k-1) = \mathbf{e}(k). \tag{7.19}$$

Equation (7.18) describes the system and the entire control diagram shown in Fig. 7.4. Restrictions that must be considered when minimizing the cost function *J* in the LQR problem are:

$$J = \frac{1}{2} \sum_{k=0}^{\infty} \left[\hat{\mathbf{x}}^{\mathsf{T}}(k) \mathbf{Q} \hat{\mathbf{x}}(k) + \hat{\mathbf{u}}^{\mathsf{T}}(k) \mathbf{R} \hat{\mathbf{u}}(k) \right] \text{ and} \tag{7.20}$$

$$\hat{\mathbf{x}}(k+1) = \hat{\mathbf{A}}_d \hat{\mathbf{x}}(k) + \hat{\mathbf{B}}_d \hat{\mathbf{u}}(k).$$

An optimal **K** matrix is obtained when the LQR problem is solved, which defines all the constants of the control diagram:

$$\mathbf{K} = \begin{bmatrix} \mathbf{K}_i & \mathbf{K}_x & \mathbf{K}_u \end{bmatrix}. \tag{7.21}$$

7.3.4. Three-Level Boost Rectifier with LQR

The small-signal state-space model (2.40) is used to solve the LQR problem in this section, such that

$$\frac{d}{dt}\begin{bmatrix} \tilde{i}_d \\ \tilde{i}_q \\ \tilde{v}_{DC} \end{bmatrix} = \begin{bmatrix} -\dfrac{R}{L} & \omega & 0 \\ -\omega & -\dfrac{R}{L} & 0 \\ -\dfrac{2v_{dss}}{CV_{DC}^*} & -\dfrac{2v_{qss}}{CV_{DC}^*} & \dfrac{2(v_{dss}i_{dss}+v_{qss}I_q^*)}{CV_{DC}^{*2}} \end{bmatrix}\begin{bmatrix} \tilde{i}_d \\ \tilde{i}_q \\ \tilde{v}_{DC} \end{bmatrix} + \begin{bmatrix} \dfrac{1}{L} & 0 \\ 0 & \dfrac{1}{L} \\ -\dfrac{2i_{dss}}{CV_{DC}^*} & -\dfrac{2I_q^*}{CV_{DC}^*} \end{bmatrix}\begin{bmatrix} \tilde{v}_d \\ \tilde{v}_q \end{bmatrix} + \begin{bmatrix} -\dfrac{1}{L} & 0 \\ 0 & 0 \\ 0 & \dfrac{2}{C} \end{bmatrix}\begin{bmatrix} \tilde{E}_L \\ \tilde{i}_{DC} \end{bmatrix}$$

$$\begin{bmatrix} \tilde{i}_q \\ \tilde{v}_{DC} \end{bmatrix} = \begin{bmatrix} 0 & 1 & 0 \\ 0 & 0 & 1 \end{bmatrix}\begin{bmatrix} \tilde{i}_d \\ \tilde{i}_q \\ \tilde{v}_{DC} \end{bmatrix}, \tag{7.22}$$

in which the state variables, the control variables and the disturbances are

$$\begin{bmatrix} \tilde{i}_d & \tilde{i}_q & \tilde{v}_{DC} \end{bmatrix}^\mathsf{T}, \quad \begin{bmatrix} \tilde{v}_d & \tilde{v}_q \end{bmatrix}^\mathsf{T}, \quad \text{and} \quad \begin{bmatrix} \tilde{E}_L & \tilde{i}_{DC} \end{bmatrix}^\mathsf{T}, \text{ respectively.} \tag{7.23}$$

According to this model, the matrices can be identified as:

$$\mathbf{A}_{\{3x3\}} = \begin{bmatrix} -\dfrac{R}{L} & \omega & 0 \\ -\omega & -\dfrac{R}{L} & 0 \\ -\dfrac{2v_{dss}}{CV_{DC}^*} & -\dfrac{2v_{qss}}{CV_{DC}^*} & \dfrac{2(v_{dss}i_{dss}+v_{qss}I_q^*)}{CV_{DC}^{*2}} \end{bmatrix}, \tag{7.24}$$

$$\mathbf{B}_{1\{3x2\}} = \begin{bmatrix} \dfrac{1}{L} & 0 \\ 0 & \dfrac{1}{L} \\ -\dfrac{2i_{dss}}{CV_{DC}^*} & -\dfrac{2I_q^*}{CV_{DC}^*} \end{bmatrix}, \quad \mathbf{B}_{2\{3x2\}} = \begin{bmatrix} -\dfrac{1}{L} & 0 \\ 0 & 0 \\ 0 & \dfrac{2}{C} \end{bmatrix}, \quad \text{and} \quad \mathbf{C}_{\{2x3\}} = \begin{bmatrix} 0 & 1 & 0 \\ 0 & 0 & 1 \end{bmatrix}.$$

The discrete matrices $\mathbf{A}_d$, $\mathbf{B}_{d1}$ and $\mathbf{B}_{d2}$ can be obtained by transforming the continuous-time description of the system into a discrete-time description by means of (7.6). Thus, a new state-space formulation is obtained, as follows:

$$
\begin{bmatrix} \Delta \mathbf{v}(k+1)_{\{2x1\}} \\ \Delta \mathbf{x}(k+1)_{\{3x1\}} \\ \Delta \mathbf{x}_u(k+1)_{\{2x1\}} \end{bmatrix} = \begin{bmatrix} \mathbf{I}_{\{2x2\}} & [-\mathbf{CA}_d]_{\{2x3\}} & [-\mathbf{CB}_{d1}]_{\{2x2\}} \\ \mathbf{0}_{\{3x2\}} & \mathbf{A}_{d\{3x3\}} & \mathbf{B}_{d1\{3x2\}} \\ \mathbf{0}_{\{2x2\}} & \mathbf{0}_{\{2x3\}} & \mathbf{0}_{\{2x2\}} \end{bmatrix} \begin{bmatrix} \Delta \mathbf{v}(k+1)_{\{2x1\}} \\ \Delta \mathbf{x}(k+1)_{\{3x1\}} \\ \Delta \mathbf{x}_u(k+1)_{\{2x1\}} \end{bmatrix} + \begin{bmatrix} \mathbf{0}_{\{2x2\}} \\ \mathbf{0}_{\{3x2\}} \\ \mathbf{I}_{\{2x2\}} \end{bmatrix} \Delta \mathbf{u}(k)_{\{2x1\}}.
$$

$$(7.25)$$

This equation matches the standard state-space formulation:

$$
\hat{\mathbf{x}}(k+1)_{\{7x1\}} = \hat{\mathbf{A}}_{d\{7x7\}} \hat{\mathbf{x}}(k)_{\{7x1\}} + \hat{\mathbf{B}}_{d\{7x2\}} \hat{\mathbf{u}}(k)_{\{2x1\}}.
$$

$$(7.26)$$

Therefore, the performance index that must be minimized is:

$$
J = \frac{1}{2} \sum_{k=0}^{\infty} \left[\hat{\mathbf{x}}^{\mathrm{T}}(k)_{\{1x7\}} \mathbf{Q}_{\{7x7\}} \hat{\mathbf{x}}(k)_{\{7x1\}} + \hat{\mathbf{u}}^{\mathrm{T}}(k)_{\{1x2\}} \mathbf{R}_{\{2x2\}} \hat{\mathbf{u}}(k)_{\{2x1\}} \right],
$$

$$(7.27)$$

and solving for the optimal problem, the matrix obtained is:

$$
\mathbf{K}_{\{2x7\}} = \begin{bmatrix} \mathbf{K}_{i\{2x2\}} & \mathbf{K}_{x\{2x3\}} & \mathbf{K}_{u\{2x2\}} \end{bmatrix}.
$$

$$(7.28)$$

7.3.5. Simulated Results

In this section, some data values are given to the power system (Fig. 7.5) in order to obtain simulated results. The values assumed are R=0.1 Ω, L=1 mH, C=1000 μF, RMS line-to-line voltage E_L=1000 V and frequency f=50 Hz. The DC-link current is i_{DC}=-100 A (rectifier operation), and the DC-link voltage reference is V_{DC}^*=1500 V. The modulation period and the sample period are T_m=0.2 ms (f_m=5 kHz).

Two cases are analyzed, unity PF operation ($I_q^* = 0$) and non-unity PF operation ($I_q^* \neq 0$).
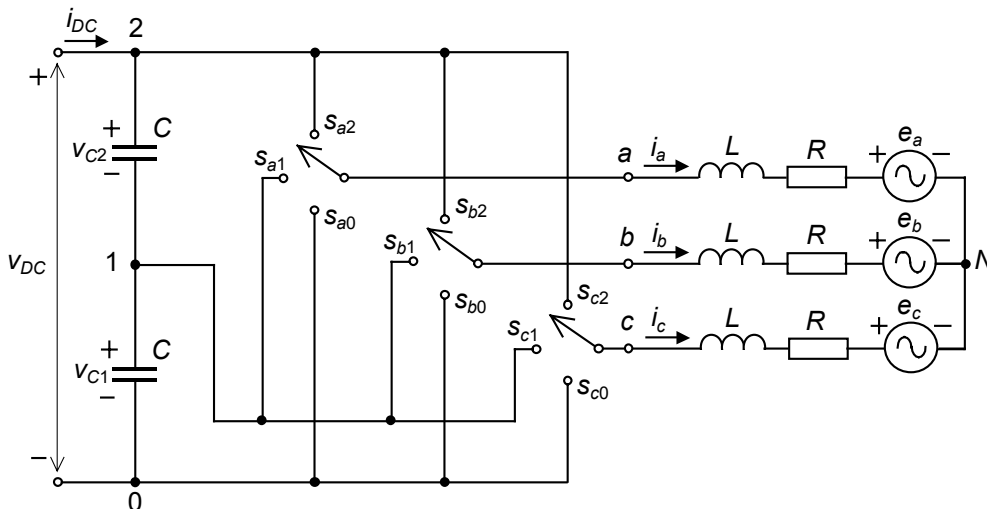

Fig. 7.5. *Three-level system to be controlled.*

7.3.5.1. Unity PF Operation

Making the reference value of the reactive current equal zero, the system operates at unity PF. The variables at the operating point are $e_{dss} = E_L = 1000\,V$, $e_{qss} = 0\,V$, $i_{qss} = I_q^* = 0\,A$, and $v_{DCss} = V_{DC}^* = 1500\,V$. The remaining values can be calculated by means of (2.37), as follows:

$$i_{dss} = \sqrt{\left(\frac{E_L}{2R}\right)^2 + \frac{V_{DC}^*}{R}i_{DCss} - I_q^{*2}} - \frac{E_L}{2R} = -152.32\,A,$$

$$v_{dss} = E_L + R\,i_{dss} - \omega L I_q^* = 984.77\,V,\ \text{ and} \tag{7.29}$$

$$v_{qss} = \omega L\,i_{dss} + R I_q^* = -47.85\,V.$$

After numerous simulations, the estimated best values for matrices **Q** and **R** are:

$$\mathbf{Q} = \begin{bmatrix} 1 & 0 & 0 & 0 & 0 & 0 & 0 \\ 0 & 1 & 0 & 0 & 0 & 0 & 0 \\ 0 & 0 & 20 & 0 & 0 & 0 & 0 \\ 0 & 0 & 0 & 20 & 0 & 0 & 0 \\ 0 & 0 & 0 & 0 & 10 & 0 & 0 \\ 0 & 0 & 0 & 0 & 0 & 1 & 0 \\ 0 & 0 & 0 & 0 & 0 & 0 & 1 \end{bmatrix} \quad \text{and} \quad \mathbf{R} = \begin{bmatrix} 1 & 0 \\ 0 & 1 \end{bmatrix}. \tag{7.30}$$

These values provide very good performance of the system in terms of achieving smooth and short transitory responses and not very strong control actions.

Solving the LQR problem for **K** obtains:

$$\mathbf{K} = \begin{bmatrix} 0.0353 & 0.4403 & 5.1131 & 0.3274 & -3.8463 & 0.7735 & 0.0407 \\ -0.4733 & 0.0325 & -0.0861 & 3.1267 & -0.3027 & -0.0180 & 0.6323 \end{bmatrix}. \tag{7.31}$$

This matrix provides all the values required for the LQR control diagram given in Fig. 7.4.

$$\mathbf{K}_i = \begin{bmatrix} 0.0353 & 0.4403 \\ -0.4733 & 0.0325 \end{bmatrix}, \ \mathbf{K}_x = \begin{bmatrix} 5.1131 & 0.3274 & -3.8463 \\ -0.0861 & 3.1267 & -0.3027 \end{bmatrix}, \tag{7.32}$$

$$\text{and } \mathbf{K}_u = \begin{bmatrix} 0.7735 & 0.0407 \\ -0.0180 & 0.6323 \end{bmatrix}.$$

The process starts in steady-state conditions where the load current is i_{DC}=-100 A. During the interval of time $[20\,ms,\,40\,ms]$, this current is perturbed, so that its value suddenly becomes -50 A.

Fig. 7.6(a) shows the total DC-link voltage (v_{DC}), the voltages of the capacitors (v_{C1} and v_{C2}), the reactive current (i_q), and the active current (i_d). Smooth peaks are produced in the voltages during current transitions. Additionally, the voltages of the capacitors are kept nearly equal, owing to proper selection of short vectors by the NTV modulation strategy. The system operates at unity PF since the reactive current is maintained near zero, even during transitions.

Utility phase voltages and currents are shown in Fig. 7.6(b). Since the conventional direction assigned to the currents is for inverter mode operation (Fig. 7.5), each current has a phase opposite to its respective phase voltage. Fig. 7.6(c) shows the trajectory of the current vector in the $\alpha\beta$ representation.
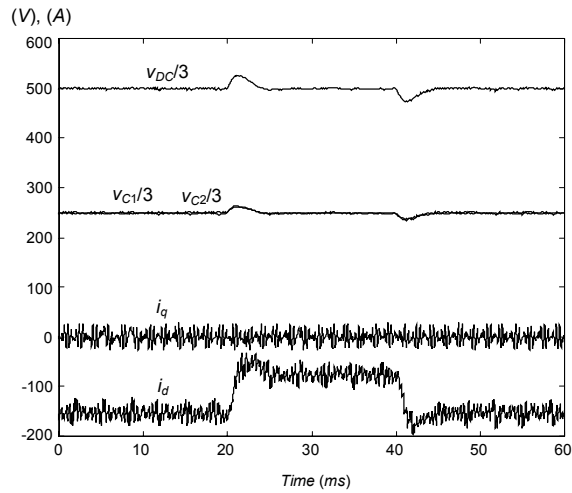
(a)
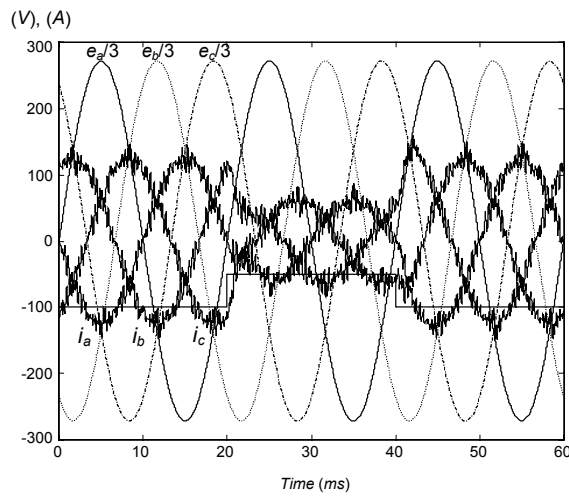
(b)
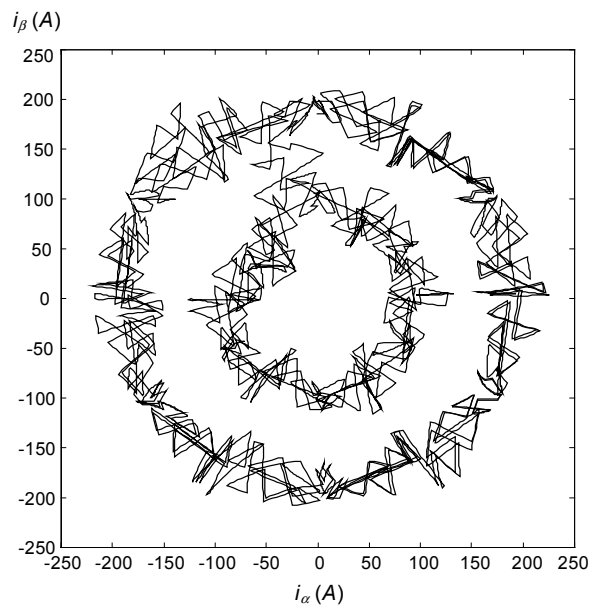
(c)

Fig. 7.6. *Simulated results for unity PF operation.*

7.3.5.2. Non-Unity PF Operation

When the system operates with non-zero reactive current (I_q*≠0), a significant NP voltage ripple may appear. Therefore, the feedforward modulation can be very useful to attenuate the effects of that oscillation.

Now, the same data values as in the previous section are used for the simulations, but the reactive current is $i_{qss} = I_q^* = 350\ A$. Therefore:

$$i_{dss} = \sqrt{\left(\frac{E_L}{2R}\right)^2 + \frac{V_{DC}^*}{R} i_{DCss} - I_q^{*2}} - \frac{E_L}{2R} = -164.97\ A,$$

$$v_{dss} = E_L + R\ i_{dss} - \omega L I_q^* = 873.55\ V \text{ , and} \tag{7.33}$$

$$v_{qss} = \omega\ L\ i_{dss} + R I_q^* = -16.83\ V.$$

Using the same weight matrices **Q** and **R** (7.30) and solving the LQR problem for **K** yields:

$$\mathbf{K} = \begin{bmatrix} 0.2088 & 0.3947 & 4.9764 & -1.2690 & -3.5860 & 0.7519 & 0.0547 \\ -0.4169 & 0.2034 & 0.4445 & 2.7260 & -1.2009 & 0.0252 & 0.6622 \end{bmatrix}. \tag{7.34}$$

Fig. 7.7 shows some waveforms for non-compensated modulation and feedforward modulation. The AC currents do not contain significant low-frequency distortion for feedforward modulation, since the $\alpha\beta$ representation of those currents is clearly circular.
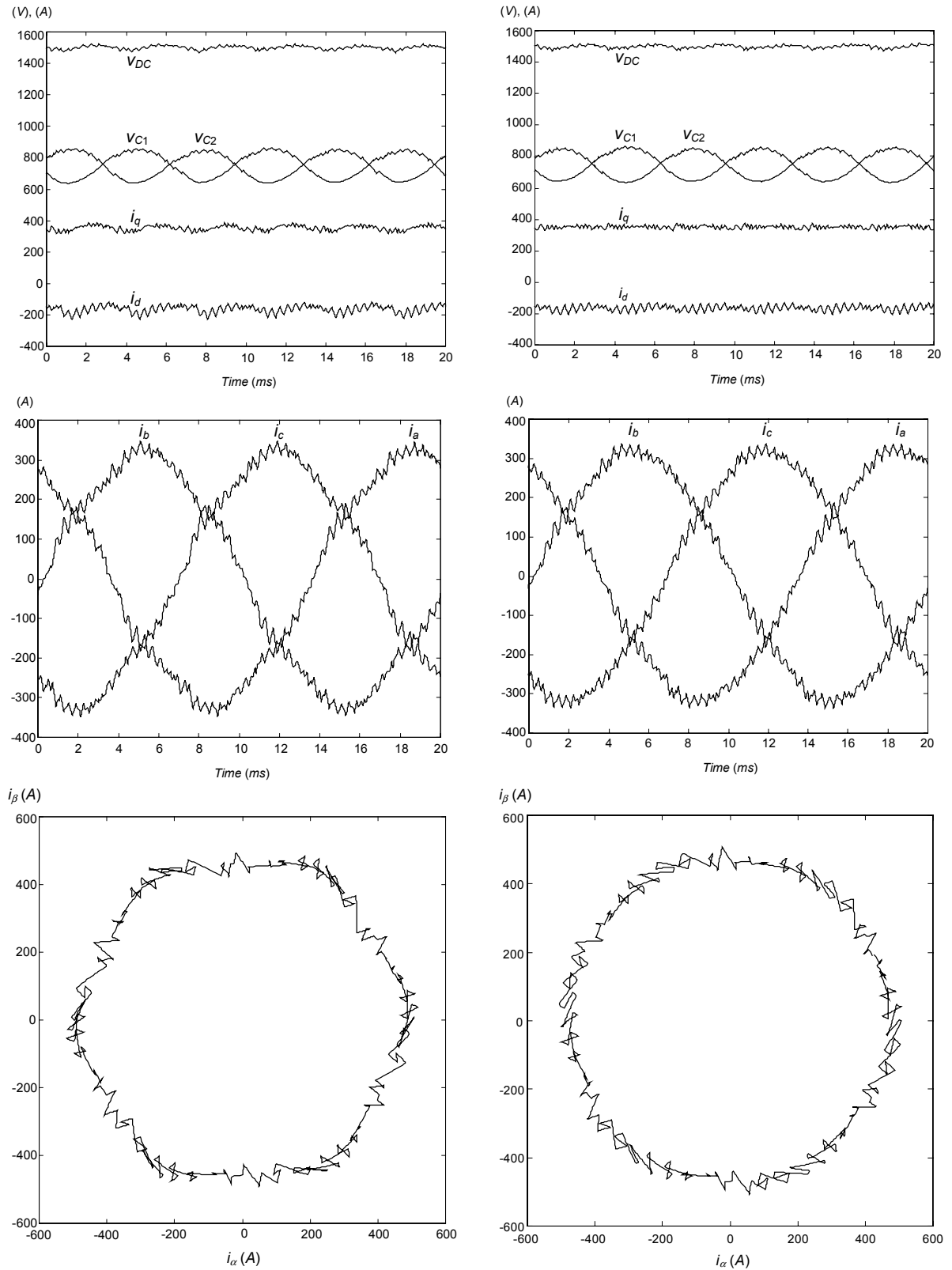
Fig. 7.7. *Simulated results for non-zero reactive current.*
Left graphics: with non-compensated NTV modulation.
Right graphics: with feedforward modulation.

7.3.5.3. Effects of NP Voltage Oscillation

One of the consequences of the NP voltage oscillation is the existence of low-frequency distortion produced in the AC currents. Feedforward modulation can attenuate such distortion; however, when the converter controls the total DC-link voltage, it will be impossible to keep this voltage at a constant level. As a consequence, the controller will introduce oscillations in the references of the transformed currents, and accordingly, distortion in the AC currents. Therefore, feedforward modulation cannot completely avoid this distortion, since it is implicit in the current references given by the controller. This statement is demonstrated in the following.
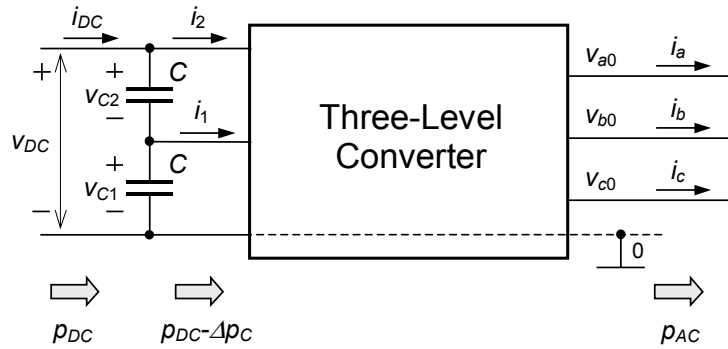
***Fig. 7.8.** Voltages and currents in the three-level system.*

Assuming local averaged variables in the analysis, the instantaneous power at the DC side and the AC side of the converter is expressed by:

$$\begin{cases} \overline{p}_{DC} = \overline{V}_{DC}\, \overline{i}_{DC} \quad \text{and} \\ \overline{p}_{AC} = \overline{V}_{a0}\, \overline{i}_a + \overline{V}_{b0}\, \overline{i}_b + \overline{V}_{c0}\, \overline{i}_c = \overline{V}_d\, \overline{i}_d + \overline{V}_q\, \overline{i}_q. \end{cases} \tag{7.35}$$

If 100% efficiency is taking into account:

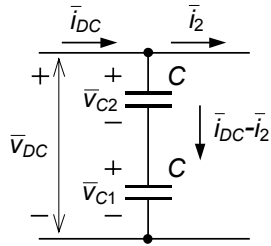$$\overline{p}_{AC} = \overline{p}_{DC} - \Delta\overline{p}_C, \tag{7.36}$$

in which $\Delta\overline{p}_C$ is related to the variation of energy in the capacitors. This term can be expressed as follows:

$$\Delta\overline{p}_C = \frac{d\overline{\varepsilon}_C}{dt} = \overline{V}_{DC}(\overline{i}_{DC} - \overline{i}_2) - \overline{V}_{C1}\overline{i}_1. \tag{7.37}$$

<u>Case 1</u>: The averaged NP current is zero ($\bar{i}_1 = 0$).

In this case, $\Delta\bar{p}_C$ becomes:

$$\Delta\bar{p}_C = \bar{V}_{DC}(\bar{i}_{DC} - \bar{i}_2) = \bar{V}_{DC}\frac{C}{2}\frac{d\bar{v}_{DC}}{dt}. \qquad (7.38)$$
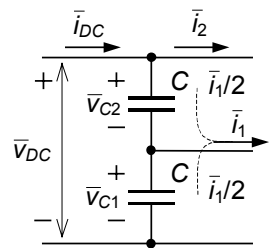
If the DC-link voltage is kept constant, $\Delta\bar{p}_C$ is zero. Thus, in accordance with (7.36), the instantaneous power p_{DC} and p_{AC} are equal. Assuming constant i_{DC} in the steady-state condition:

$$\bar{p}_{AC} = \bar{p}_{DC} = \bar{V}_{DC}\bar{i}_{DC} = ct. \qquad (7.39)$$

As a result, the instantaneous power in the AC side is also constant. Therefore, the AC currents will not contain low-frequency distortion. In this case, the controller can achieve the constant DC-link voltage and the AC currents with no distortion simultaneously.

<u>Case 2</u>: The averaged NP current is not constant ($\bar{i}_1 \neq 0$).

Assuming that the controller can achieve the constant DC-link voltage, the current in the upper capacitor becomes $\bar{i}_1/2$. As a result, $\Delta\bar{p}_C$ is:

$$\Delta\bar{p}_C = \bar{V}_{DC}\frac{\bar{i}_1}{2} - \bar{V}_{C1}\bar{i}_1 = \left(\frac{\bar{V}_{DC}}{2} - 2C\frac{d\bar{i}_1}{dt}\right)\bar{i}_1. \qquad (7.40)$$

In this case, $\bar{p}_{DC}$ and $\bar{p}_{AC}$ are not equal. Assuming constant $\bar{i}_{DC}$ in the steady-state condition:

$$\begin{cases} \bar{p}_{DC} = \bar{V}_{DC}\,\bar{i}_{DC} = ct. \text{ and} \\ \bar{p}_{AC} = f(\bar{i}_1) \neq ct. \end{cases} \qquad (7.41)$$

As a result, $\overline{p}_{AC}$ is not constant and the AC currents will contain low-frequency distortion. Thus, the controller cannot achieve the constant DC-link voltage and the non-distortion in the AC currents simultaneously.

In conclusion, if the local averaged NP current is not zero, it is not possible to keep the constant DC-link voltage without introducing fluctuations in the instantaneous AC power (i. e., distortion in the AC currents). Therefore, although the simulated results obtained by feedforward modulation in the previous section show almost constant DC-link voltage and sinusoidal currents, it is impossible to completely achieve both objectives when the averaged NP current is not confined to zero.

7.3.6. Experimental Results

The proposed LQR controller has been programmed in the DSP of the SMES system. The data used for the experimental results are R=0.1 Ω, L=0.5 mH, C=1650 μF, E_L= 60 V and frequency f=60 Hz. The reference values of the LQR control are $I_q^* = 0\ A$ and $V_{DC}^* = 100\ V$, and the sample and modulation periods are T_s=T_m= 50 μs (f_s=20 kHz). The DC-link current is $i_{DC} = -4\ A$ (rectifier mode). Therefore, the values of the variables at the operating point are:

$$e_{dss} = E_L = 60\ V, \quad e_{qss} = 0\ V, \quad i_{qss} = I_q^* = 0\ A, \quad v_{DCss} = V_{DC}^* = 100\ V, \quad (7.42)$$

$$i_{dss} = \sqrt{\left(\frac{E_L}{2R}\right)^2 + \frac{V_{DC}^*}{R} i_{DCss} - I_q^{*2}} - \frac{E_L}{2R} = -6.7424\ A,$$

$$v_{dss} = E_L + R\ i_{dss} - \omega L I_q^* = 59.3258\ V, \text{ and}$$

$$v_{qss} = \omega\ L\ i_{dss} + R I_q^* = -1.2709\ V.$$

In this case, the estimated best values for matrices **Q** and **R** are

$$\mathbf{Q} = \begin{bmatrix} 1 & 0 & 0 & 0 & 0 & 0 & 0 \\ 0 & 1 & 0 & 0 & 0 & 0 & 0 \\ 0 & 0 & 100 & 0 & 0 & 0 & 0 \\ 0 & 0 & 0 & 100 & 0 & 0 & 0 \\ 0 & 0 & 0 & 0 & 10 & 0 & 0 \\ 0 & 0 & 0 & 0 & 0 & 1 & 0 \\ 0 & 0 & 0 & 0 & 0 & 0 & 1 \end{bmatrix} \quad \text{and} \quad \mathbf{R} = \begin{bmatrix} 1 & 0 \\ 0 & 1 \end{bmatrix}, \quad (7.43)$$

which results with the following components of matrix **K**:

$$\mathbf{K}_i = \begin{bmatrix} 0.0123 & 0.4820 \\ -0.4792 & 0.0124 \end{bmatrix}, \quad \mathbf{K}_x = \begin{bmatrix} 6.4488 & 0.1443 & -12.8447 \\ -0.1302 & 5.7957 & -0.3325 \end{bmatrix}, \tag{7.44}$$

$$\text{and } \mathbf{K}_u = \begin{bmatrix} 0.5725 & 0.0090 \\ -0.0096 & 0.5826 \end{bmatrix}.$$

For the experimental results, the process starts with no load connected to the DC link. Then, turning on the switch in Fig. 7.9 a 25-ohm resistive load is connected.
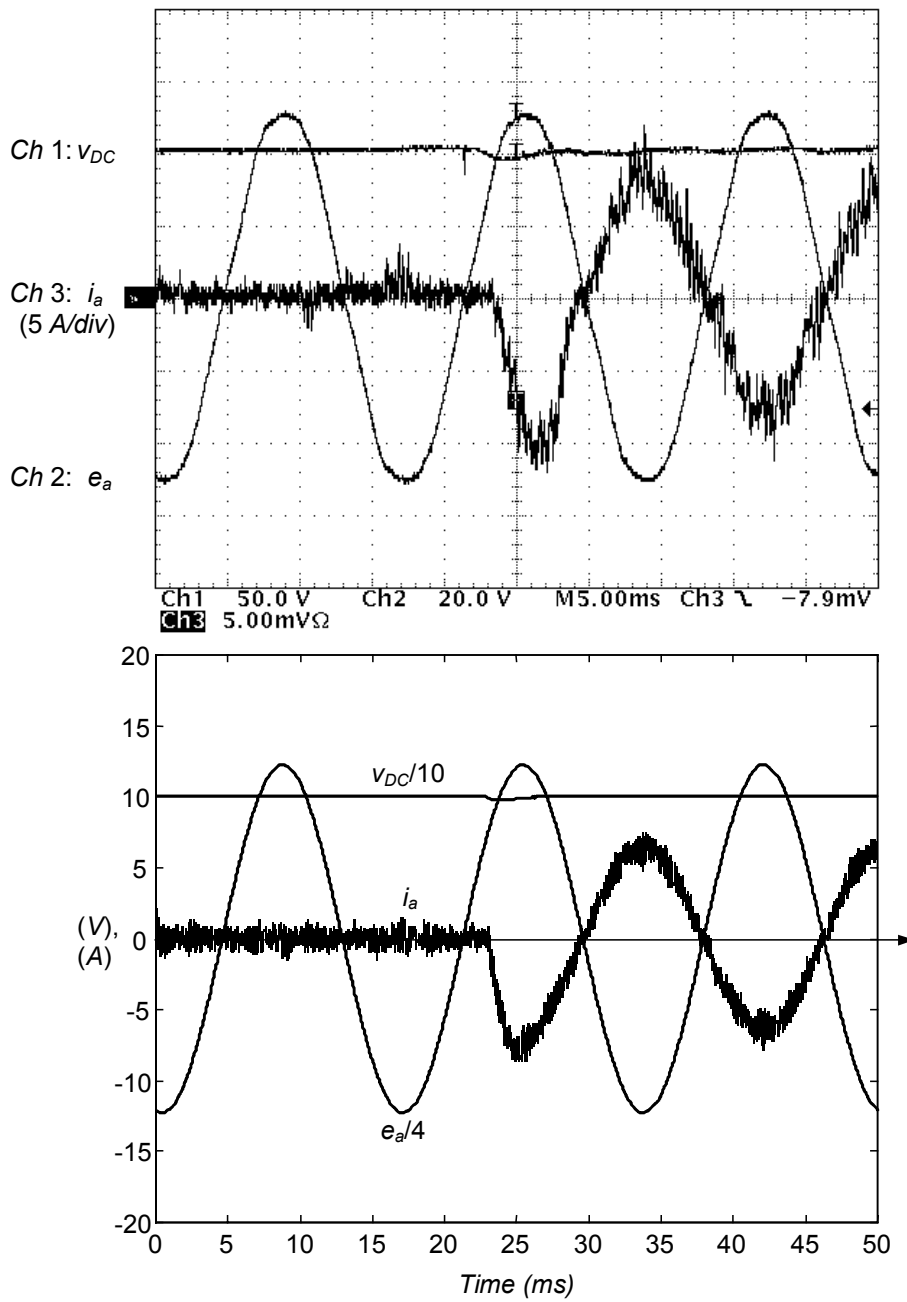
Fig. 7.10 shows the DC-link voltage (v_{DC}), a utility phase voltage (e_a) and a phase current (i_a). Fig. 7.11 also includes a line-to-line voltage of the converter (v_{ab}). The controller adjusts the amplitude of the AC currents to achieve constant DC-link voltage, and the phase of these currents is such that the system operates at unity PF. Besides, the LQR loop provides very good dynamic performance for the system in such a transitory process.

Fig. 7.12 shows the voltages of the DC-link capacitors (v_{C1}, v_{C2}) and the dq-transformed currents (i_d, i_q) during the connection and disconnection of the load. The variables are quickly stabilized after some smooth oscillation during the connection of the load.
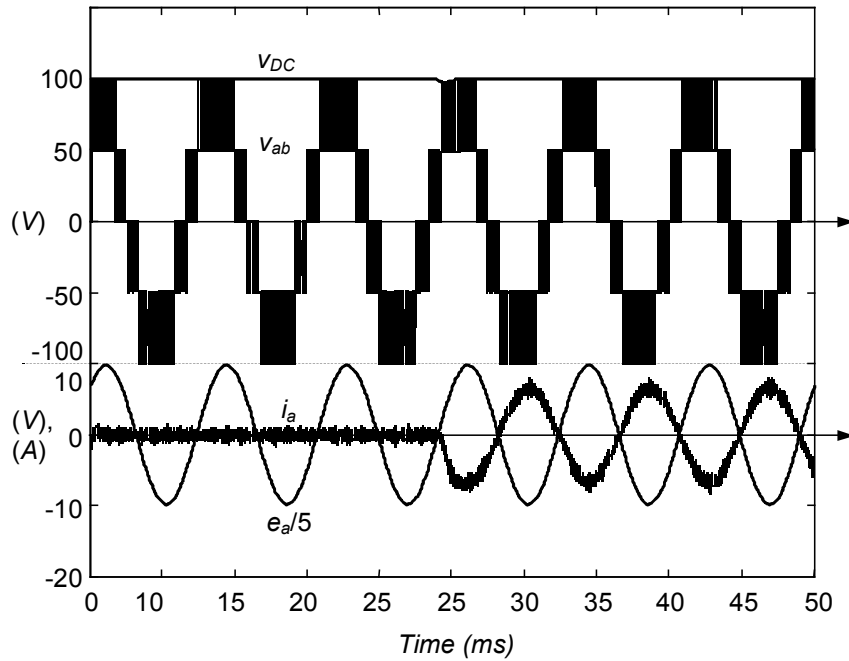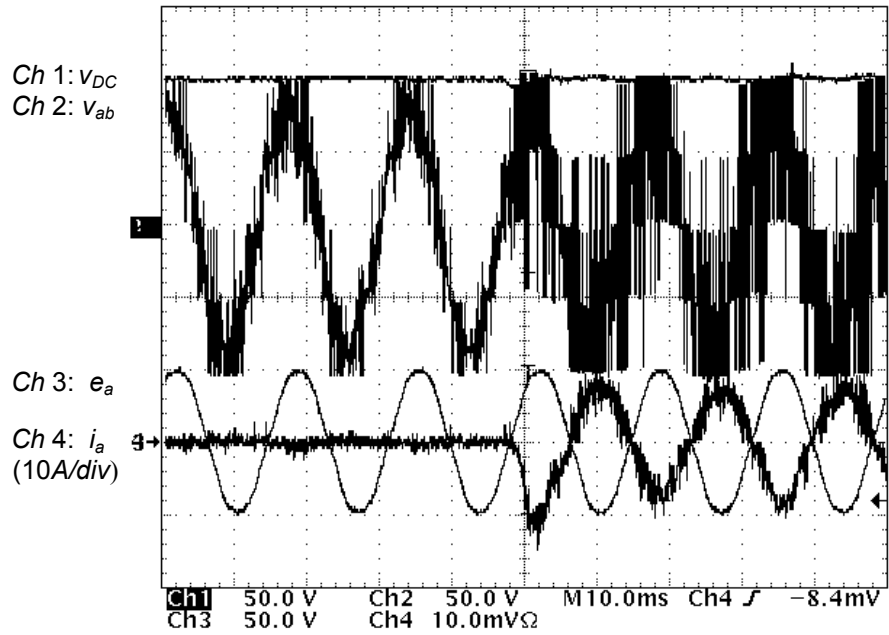
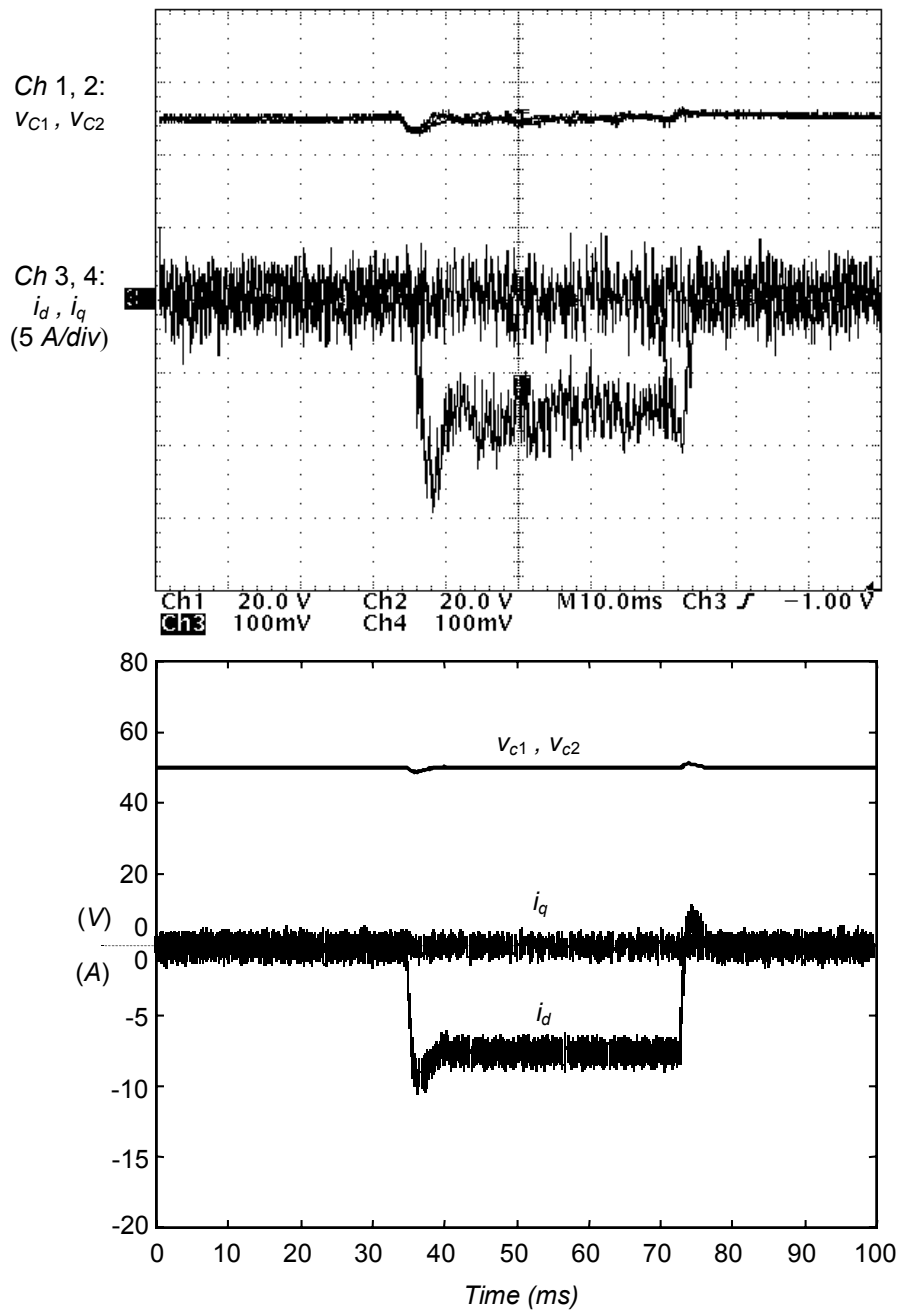All of the shown experimental results are also corroborated by simulation.
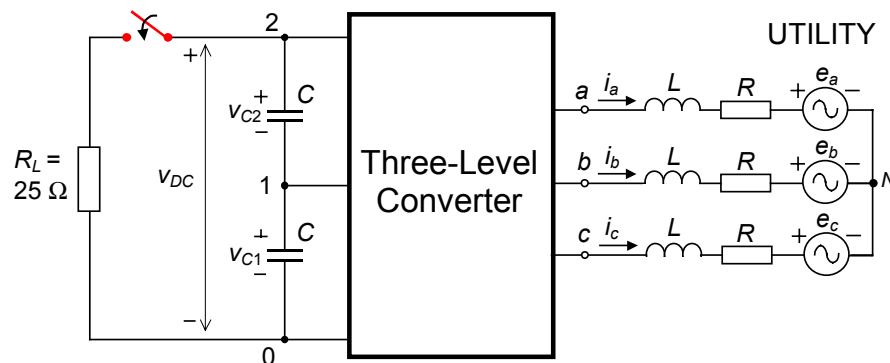
***Fig. 7.9.** System considered for the experimental results.*

Fig. 7.10. *DC-link voltage (v$_{DC}$), a utility phase voltage (e$_a$) and a phase current (i$_a$) during the transitory process of turning the switch on.*

Fig. 7.11. Line-to-line voltage of the converter (v_ab) during a process similar to that shown in Fig. 7.10.

Fig. 7.12. *Voltages of the DC-link capacitors (v_{C1} and v_{C2}) and dq-transformed currents (i_d and i_q) during the connection and disconnection of the load.*

7.4. Conclusions of the Chapter

In this chapter, an optimal multivariable controller is analyzed, which includes integral actuation and considers intrinsic delay of one modulation period in the control variables. A similar control diagram is used in [A50]; however, that approach performs NP-current control by means of the LQR loop itself. As a result, the model of the converter used for the control is more complicated, which eventually generates a matrix **K** of 3x10 elements instead of the matrix **K** of 2x7 elements obtained in the present approach. Additionally, the instantaneous NP current reference given by the controller to the modulation stage is not achieved due to nonlinear performance of the modulator. This nonlinearity is not considered in the LQR control loop; therefore, the NP current is not optimally controlled.

In this approach, the NP voltage balance is carried out by the modulation stage instead of the controller. Since the best NTVs are selected per each modulation period, "optimal" NP balancing results are achieved.

Simulated and experimental results validate very good dynamic and static performance of the system. Non low-frequency NP voltage oscillation practically appears when the converter operates as a boost rectifier with unity PF ($I_q^* = 0$).

When there is NP voltage oscillation due to non-unity PF ($I_q^* \neq 0$) operation, some simulated results show significant improvement in AC current distortion and DC-link voltage oscillation thanks to feedforward modulation. However, such improvements cannot completely avoid low-frequency distortion, as has been mathematically demonstrated.